THERMAL HELIUM DESORPTION OF HELIUM-IMPLANTED IRON—D. Xu, T. Bus, S. C. Glade, and B. D. Wirth (University of California, Berkeley)

OBJECTIVE

The objective of this work is to understand the kinetics and energetics of helium in iron implanted with He ions at different energies and fluences.

SUMMARY

Following the last report, we have performed new implantations at energies lower than 100 keV, with an aim of reducing the penetration depth of helium atoms and the structural damage, and thus reducing the He-point defect interaction complexity during desorption experiments. Initial measurements on the new samples have revealed a large number of desorption peaks within both the bcc and fcc temperature ranges. These peaks are well fit with first order reaction kinetics, which reveal activation energies ranging from ~1.9 to ~3.5 eV. The number and the relative intensities of detected desorption peaks within the bcc temperature range appear to increase with decreasing implantation energy. Previously reported spurious peaks and a non-1st-order sharp peak are now better understood and described in the current report.

PROGRESS AND STATUS

Introduction

Helium effects on the microstructure and mechanical properties are among the most critical subjects in fusion materials research. It has been shown that implanted or internally produced (by neutron radiation) helium can cause formation of voids and bubbles in the materials and thus result in significant mechanical property degradation [1–4]. A crucial aspect, therefore, is to understand how helium atoms migrate and are trapped by microstructural features in irradiated materials. While a large amount of theory, modeling and experimental research has been performed in the past years, the understanding of this problem is still far from complete.

In iron and ferritic alloys, computer simulations have been performed on defect production in collision cascades during helium injection [5], effect of He-vacancy complexes on the mechanical properties [6], thermal stability of He-vacancy and/or He/self-interstitial-atom (SIA) clusters [7–10], helium clustering at dislocations [11,12], and the He-grain boundary interaction [13–14]. Experimentally, nuclear reaction depth profiling [15], transmission electron microscopy [16], positron annihilation lifetime and coincidence Doppler broadening (CDB) techniques [17,18] and thermal helium desorption spectrometry (THDS) [7,19–20] have been used to study the He migration and He-induced defect clusters in iron.

Despite the above works, there are still many unresolved questions regarding the helium behavior in iron. For example, for the dissociation of the simple substitutional helium (i.e., HeV); different researchers have reported very different values of activation energy, such as 3.9 eV by v.d. Berg et al. [11] and Morishita et al. [7,8], 2.4 eV by Fu et al. [10], and even 1.4 eV by Vassen et al. [20]. The current knowledge about helium behavior in iron and ferritic alloys remains incomplete and is certainly less than necessary to establish a predictive model for the performance of these materials in future fusion reactors.

In our previous report [21], preliminary work on the THDS study of the kinetics and energetics of helium in iron implanted with 100 keV He to three different fluences, $1x10^{11}$, $1x10^{13}$, and $1x10^{15}$ He/cm^2 was presented. In that report, it was observed that certain unknown spurious peaks which were apparently not related to the desorption of implanted helium appeared on the measured helium signals from all the 100 keV samples. From the two lower fluence ($1x10^{11}$ and $1x10^{13}$ He/cm^2) samples, particularly, no clear signals were observed that could be unambiguously associated with real desorption of implanted helium within the entire temperature range of measurement (from room temperature up to 1330°C). For the

highest fluence ($1x10^{15}$ He/cm^2) sample, however, two major real desorption events were observed with the first event peaking at ~1017°C (upon continuous heating at a rate of 1 K/s) and the second starting at ~1100°C but not ending even up to the upper limit of the measurement temperature (i.e.,1330°C). Detailed kinetic analysis showed that the low temperature desorption event of the 100 keV and $1x10^{15}$ He/cm^2 sample consists of two components (or sub-events), one with a broad peak and the other with a sharp peak. The broad component can be described by 1st-order kinetics using either conventional reaction model or Johnson-Mehl-Avrami (JMA) model, while the sharp component can only be described by a high (n ~ 5.8) order JMA model. It was also observed that a similarly sharp desorption event appeared during immediate cooling from 1330°C at the end of first heating ramp and even during subsequent re-heating and re-cooling of the 100 keV and $1x10^{15}$ He/cm^2 sample. Only after the sample was held isothermally at a very high (1330°C) temperature for a long time (~30 min) did the event disappear completely during immediate cooling and subsequent re-cycling.

Following this previous report, we have performed new implantations at energies lower than the previous 100 keV. Some of the new samples have been measured and their data has been analyzed which has yielded new information, particularly for the bcc-iron temperature range, as we will elaborate in the following.

Instrumentation

Figure 1 is a picture of the THDS system at University of California, Berkeley [22]. The construction and the operating principle have been explained in detail in the previous report [21]. Briefly, however, under the dynamic operating mode, the system measures the instantaneous gas partial current (I) by a quadrupole mass spectrometer which can be converted easily to the instantaneous desorption rate ($d\overline{N}/dt$) of that gas using the proportional relation: $d\overline{N}/dt \propto (P - P_{base}) \propto (I - I_{base})$. The proportion coefficient can be determined using a calibration procedure [21].

Fig. 1. Picture of the Berkeley THDS instrument.

Theory

After implantation, helium atoms are trapped by various microstructural defects inside the implanted material. The trapping defects include those created during implantation such as vacancies, self-interstitial-atoms (SIAs) and their clusters, and those already existent prior to the implantation such as thermal vacancies, dislocations, grain boundaries, impurities, etc. During subsequent thermal annealing,

three different kinetic processes may occur: diffusion, detrapping and retrapping. A general description of the overall kinetics can be represented by (in 1-D case):

$$\vec{J}(x,t) = -\sum_i D_i(t)\vec{\nabla}C_{mob,i}(x,t) \tag{1}$$

$$\frac{\partial C_{mob}(x,t)}{\partial t} = -\vec{\nabla}\vec{J}(x,t) + \sum_j \frac{\partial C^j_{detrap}(x,t)}{\partial t} - \sum_k \frac{\partial C^k_{retrap}(x,t)}{\partial t} \tag{2}$$

where the first summation (in Eq. (1)) refers to the diffusion by different mechanisms, the second to the detrapping from different traps, and the third to the retrapping by different traps. Assuming that the diffusion of mobile helium atoms is fast until they are retrapped or reach the sample surfaces (i.e., neglecting the slow diffusion through the collective movement of a helium-containing trap which might happen if the migration energy of the trap as a whole is much lower than its dissociation energy), then the total number of mobile helium atoms inside the sample remains very low, and we have approximately (where A is surface area)

$$\frac{\partial \int C_{mob}(x,t)Adx}{\partial t} \sim 0\,. \tag{3}$$

Integrating Eq. (2) over the length of the sample then yields

$$AJ_{tot} = A[J(0,t) + J(l,t)] \sim \sum_j \frac{\partial \int C^j_{detrap}(x,t)Adx}{\partial t} - \sum_k \frac{\partial \int C^k_{retrap}(x,t)Adx}{\partial t} \tag{4}$$

which means the instantaneous total outflux through the two surfaces is linearly related to the instantaneous detrapping (dissociation) and retrapping rates. Therefore, by measuring the total outflux (i.e., desorption signal), one can easily obtain information about the detrapping and retrapping kinetics inside the sample.

It has been reported that the interaction (detrapping and retrapping) between inert gas atoms and microstructural defects generally obeys the first order chemical reaction model, i.e.,

$$\frac{\partial}{\partial t}C^i_{detrap} = (C^i_0 - C^i_{detrap})\nu_i \exp(-\frac{E^{D,i}}{k_B T}), \tag{5}$$

where $E^{D,i}$ is the activation energy for the detrapping (dissociation) from the *i*th trap type. Then we expect to be able to derive the activation energies $E^{D,i}$, as well as the initial concentration C^i_0 and the attempt frequency ν_i of various traps (defects) from desorption signals.

However, as we see from Eq. (4), the measured desorption signals from THDS experiments may have contributions from both detrapping and retrapping, which can make the data analysis very difficult since, with strong interference of retrapping, some of the detrapping events will not be detected at all. Therefore, in order to extract the kinetic parameters more reliably and easily, we shall minimize the probability of retrapping of the detrapped helium atoms before they diffuse to the surfaces. This can be done by lowering the implantation energy which simultaneously has two positive effects: reducing the penetration

depth of helium (so that the diffusion path across the damaged layer is shorter) and reducing the amount of damage (so that the number of potential retrapping sites is lower).

Results and Discussion

TRIM/SRIM calculations

TRIM (SRIM 2003) software [23] was used to calculate the damage and helium concentration profiles with respect to depth for 5, 20, and 100 keV (as shown in Fig. 2, from left to right) helium implantations in iron at a common fluence of $1x10^{15}$ He/cm^2. Helium peak concentration depth is determined to be 26, 96, 335 nm, respectively, in the order of increasing implantation energy. The number of vacancies created per helium is 20, 50, and 87. It is clear that as the implantation energy increases the penetration depth of helium and the average damage produced per helium both increase. For the reasons discussed earlier, we shall expect less interference of retrapping with our desorption signals.

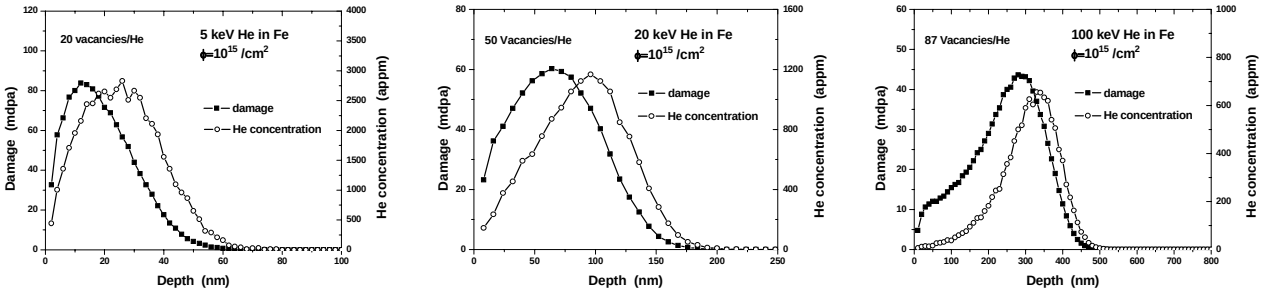

Fig. 2. (from left to right) Damage and helium concentration vs. depth for 5, 20, and 100 keV helium implantations in iron. The fluence used is $1x10^{15}$ He/cm^2 for all the three energies.

Based on the calculation and previous experience that signals from a sample with a fluence below $1x10^{13}$ He/cm^2 might be too difficult to measure using our system, we have performed new implantations with 9 new combinations of energy and fluence: 5, 10, and 20 keV for energy vs. $1x10^{13}$, $1x10^{14}$, and $1x10^{15}$ He/cm^2 for fluence. At present, we have performed measurements and data analysis on some of the newly implanted samples, while the rest of the new samples will be studied soon.

100 keV and $1x10^{15}$ He/cm^2 helium implanted iron

We shall briefly recall some of the THDS signals presented in the last report [21]. Figure 3 (left) shows the helium signal measured by the mass spectrometer from a 100 keV and 1×10^{15} ion/cm^2 helium implanted iron, and shows certain 'spurious peaks' (marked by the oval in the figure). They are considered not real desorption peaks of implanted helium but 'spurious peaks' based on two facts: (1) these peaks not only appeared in the He channel but also in other channels such as the N_2 channel as well as in the total pressure (2) these peaks were also observed even during an experiment on a non-implanted iron (shown in Fig. 3 right).

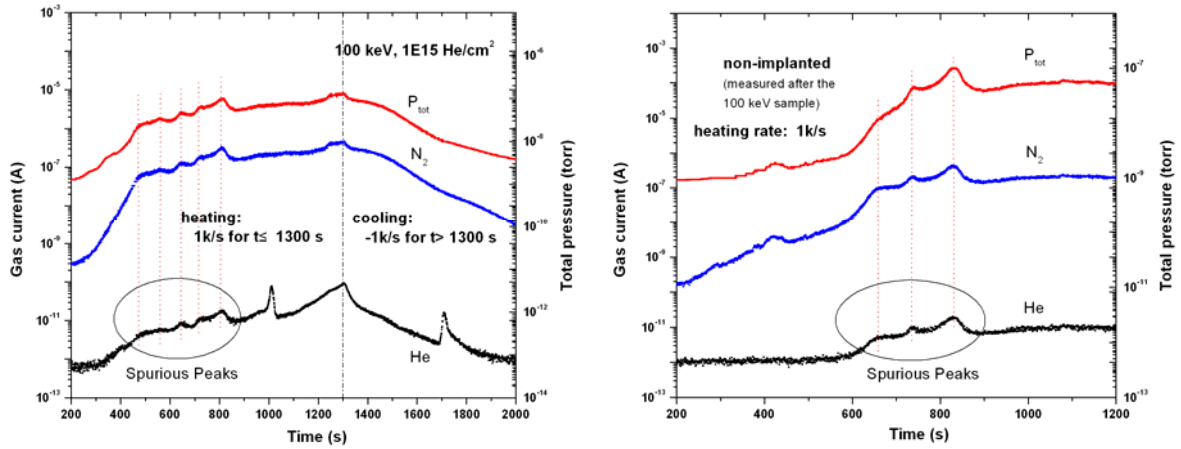

Fig. 3. Left: total pressure (measured by an ion gauge) and N_2 and He gas current (measured by a mass spectrometer) recorded during a THDS experiment on an iron sample implanted with 100 keV helium ion to a fluence of 1×10^{15} He/cm^2; right: total pressure and N_2 and He gas current recorded during a THDS experiment on non-implanted iron following the experiment shown on the left.

Besides these obvious 'spurious peaks', there is essentially no real desorption signal from the 100 keV and 1×10^{15} He/cm^2 sample that can be clearly identified below 912°C—the ideal transition temperature between alpha (bcc) and gamma (fcc) iron. Above 912°C and during subsequent cooling, as we discussed in the Introduction, certain major events distinguish the He channel from other channels (as well as distinguishing the implanted sample from the non-implanted sample) and thus should be considered as real desorption signals of implanted helium.

5 keV and 1x10^{15} He/cm^2 helium implanted iron

Figure 4 (left) shows the signals recorded during a similar THDS experiment on a newly implanted 5keV and 1x10^{15} He/cm^2 sample. The thermal scheme used was 1k/s heating up to 1330°C followed by 1k/s cooling immediately after. In the high temperature (above 912°C) regime during heating as well as in the cooling process, we see clearly different features in the He channel than in other channels, as for the case of the previous 100 keV and 1×10^{15} He/cm^2 sample. Therefore, we consider these high temperature helium signals are at least mostly, if not all, real desorption signals. However, two noticeable differences between the 5 keV sample and the 100 keV sample in this regime should be pointed out: (1) the He desorption rate already starts to drop after 1274°C (before cooling starts) for the 5 keV sample while it is still increasing at 1300°C where cooling starts for the 100 keV sample and (2) the relative intensity and thus the integrated area underneath (corresponding to the number of desorbed helium in an event) of the sharp peak around 1000-1080°C with respect to those of the even higher temperature (>1100°C) signal are larger for the 5 keV than for the 100 keV sample.

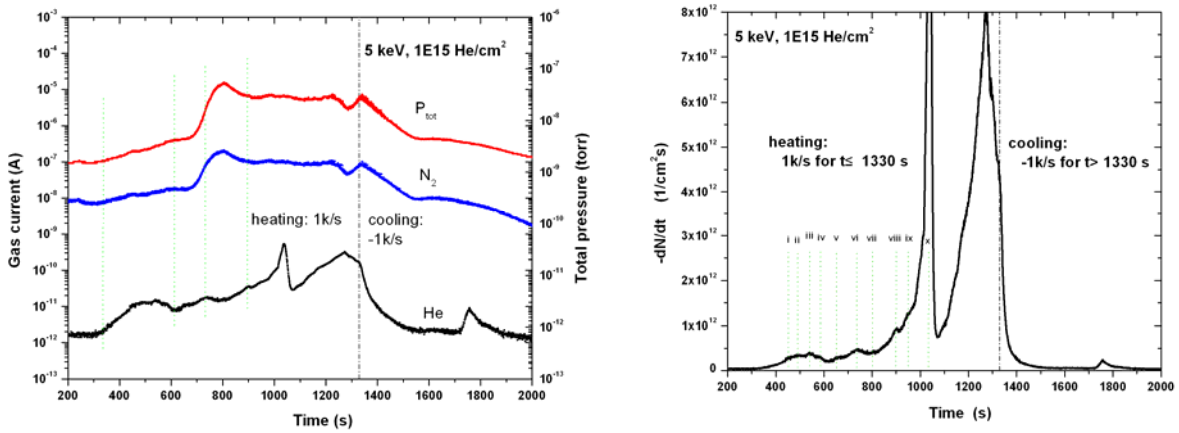

Fig. 4. Left: total pressure and N_2 and He gas current recorded during a THDS experiment on a 5keV and 1x10^{15} He/cm^2 implanted iron; Right: linearly scaled desorption rate of the 5keV and 1x10^{15} He/cm^2 sample converted from the He gas current shown on the left.

In the low temperature (below 912°C) regime during heating, we can also identify a series of small peaks on the helium signal recorded for the 5 keV sample. But what makes the 5 keV sample different from the previous 100 keV sample in this regime is that these small peaks for the new sample only appeared in the helium channel but not in other channels or in system pressure. Therefore, we consider these low temperature peaks for the 5 keV sample as real desorption signals of implanted helium.

The right of Fig. 4 shows the converted desorption rate of helium from the 5keV and 1x10^{15} He/cm^2 sample with 10 peaks denoted, including the sharp peak above 1000°C. Since most of the present simulation of helium behavior has been performed in bcc iron, and because of the unknown complexities following the bcc to fcc structural transition, we are most interested in analyzing the low temperature signals than the high temperature ones.

Since previous studies (e.g., [24]) have shown that inert gas dissociation from traps generally follows the first order reaction kinetic model, we can first base our data analysis on this assumption. In the model, the desorption rate (in terms of number per unit time) is proportional to the remaining number of helium atoms in the particular type of traps, i.e.,

$$dN/dt = -K_0 \exp(-Q/K_B T) * N \,, \tag{6}$$

where K_0 is the attempt frequency, usually on the order of 10^{13} /s, K_B is the Boltzmann constant, Q is the activation energy for the given type of traps. In comparison with Eqs. (4) and (5), Eq. (6) is actually a spatially integrated form of the concentration-represented version of the model. The temporal integration of Eq. (6) then gives,

$$N = N_0 \exp\left[-\int_0^t K_0 \exp(-Q/K_B T)dt\right]. \tag{7}$$

By virtue of Eq. (6) and Eq. (7), using three parameters, namely, K_0, Q, and N_0 for each of the identifiable desorption events, and summing all the individual desorption rates up, one can in principle fit the measured desorption rate numerically and thus determine the best values of the parameters for each individual event.

To facilitate the data fitting, we shall make initial estimates for the parameters for each event. The first step is to identify the peak positions T_p (as denoted on the right of Fig. 4). Second, we calculate Q according to the following equation

$$\ln(\beta / T_p^{\,2}) = -Q / K_B T_p + \ln(K_0 K_B / Q), \tag{8}$$

which is derived by solving the equation $d^2N/dt^2 = 0$ under the constant rate ramping condition (i.e., $dT/dt = \beta$) (note that we seemingly need to know K_0 in order to calculate Q, however, the dependence of Q on K_0 is actually fairly weak around $K_0 = 10^{13}$ /s; hence we can first estimate Q using this particular value of K_0). Third, the initial number of atoms N_0 can be estimated from the peak height (matching the calculated and the experimental heights for each peak).

Figure 5 displays the experimentally measured and numerically simulated (according to first order reaction model) helium desorption rates together with the individual desorption events/components. The agreement between the measured and the simulated desorption rates is excellent up to ~1000ºC where the non-1st-order sharp signal starts to dominate. The fitting-optimized activation energies Q for the individual events are listed in Table 1, together with the corresponding Q_{corr} values which were calculated from Eq. (8) using corrected peak positions. The correction to the peak positions will be explained later.

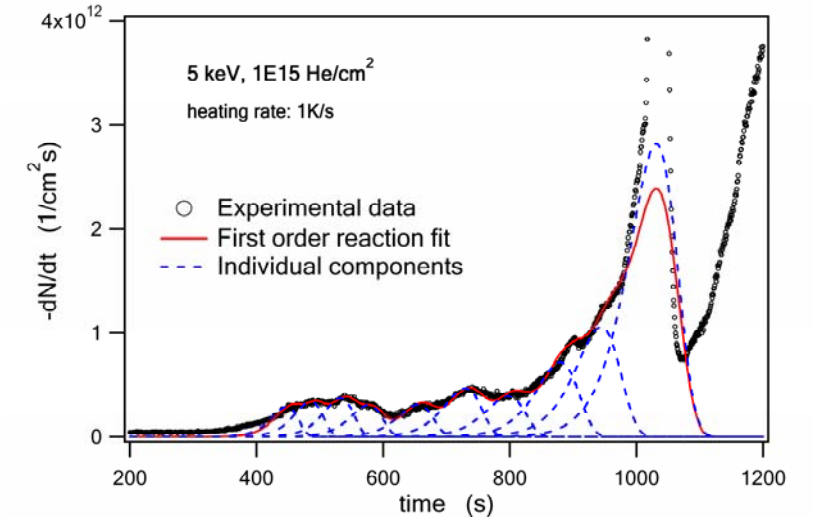

Fig. 5. Experimentally measured (circles) and numerically simulated (according to first order reaction model) (red solid line) helium desorption rates together with the individual desorption events (blue dashed line).

Table 1. Activation energies Q determined through curve fitting, and Q_{corr} calculated from Eq. (8) using peak positions corrected according to alpha to gamma transition temperature, for the 5 keV and 1×10^{15} He/cm^2 iron.

	I	II	III	IV	V	VI	VII	VIII	IX	X
Q (eV)	2.1	2.2	2.3	2.5	2.7	2.9	3.1	3.4	3.5	3.7
Q_{corr} (eV)	1.85	1.9	2.1	2.2	2.4	2.7	2.9	3.2	3.3	3.5

20 keV and 1x10^{15} He/cm^2 helium implanted iron

We have also measured and analyzed 20 keV and 1x10^{15} ion/cm^2 helium implanted iron. Shown on the left of Fig. 6 are the recorded total pressure and N_2 and He gas current during the experiment using the same thermal cycling scheme as for the 5 keV and 1x10^{15} ion/cm^2 sample.

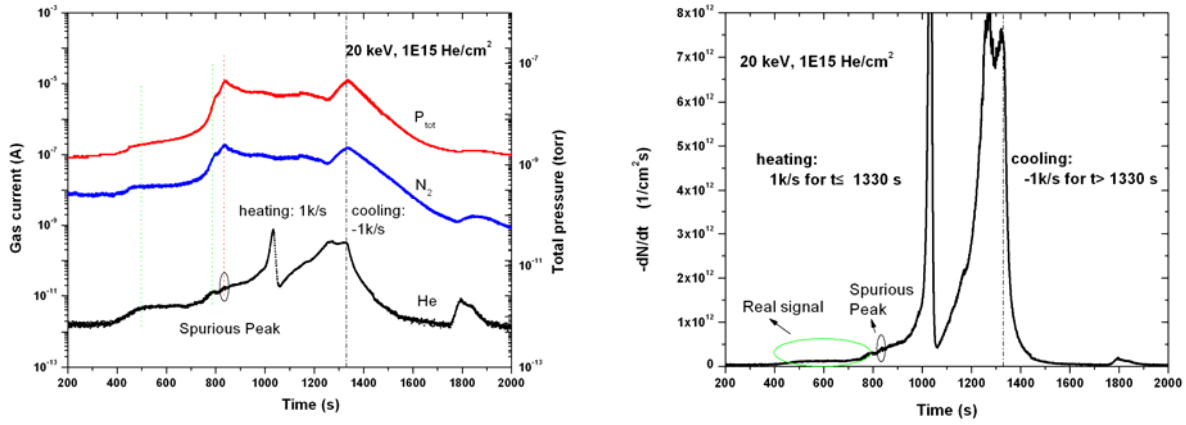

Fig. 6. Left: total pressure and N_2 and He gas current recorded during a THDS experiment on a 20keV and 1x10^{15} He/cm^2 implanted iron; Right: linearly scaled desorption rate of the 20keV and 1x10^{15} He/cm^2 sample converted from the He current shown on the left.

In the high temperature regime (above 912ºC) during heating and during cooling, we again see the helium signal distinct from N_2 or system pressure indicating that the helium signal in this regime is mostly a real desorption signal from implanted helium. Comparing with the high temperature helium signal from the 100 keV sample, we can still see the two differences we pointed out earlier when we compared the 5 keV sample with 100 keV sample, although they are more subtle here.

In the low temperature regime (below 912ºC) during heating, we see (Fig. 6, left) an initial rise in helium signal at ~390ºC followed by a plateau extending from ~500ºC to ~680ºC after which a few small peaks can be identified. Although there are also an initial rise and a plateau in N_2 channel and the system pressure, the positions of the rising and leveling-off points are clearly different from those for the helium signal. Thus we can also consider the helium signal of the 20 keV sample in this regime mostly a real desorption signal with only one peak possibly being spurious as marked out with the vertical oval in Fig. 6.

Since it is not easy to clearly identify individual peak positions from the measured desorption signal of the 20 keV sample, we choose to start with the peak positions and activation energies previously obtained from the 5 keV sample. It appears, as shown in Fig. 7, that with the same number of component events we can only get a fair agreement between the simulated and the measured signal for the 20 keV sample. More specifically, there are always a few separated intervals on the simulated curve for this 20 keV sample, including one near the marked ‘spurious peak,’ that cannot match the measured signal well.

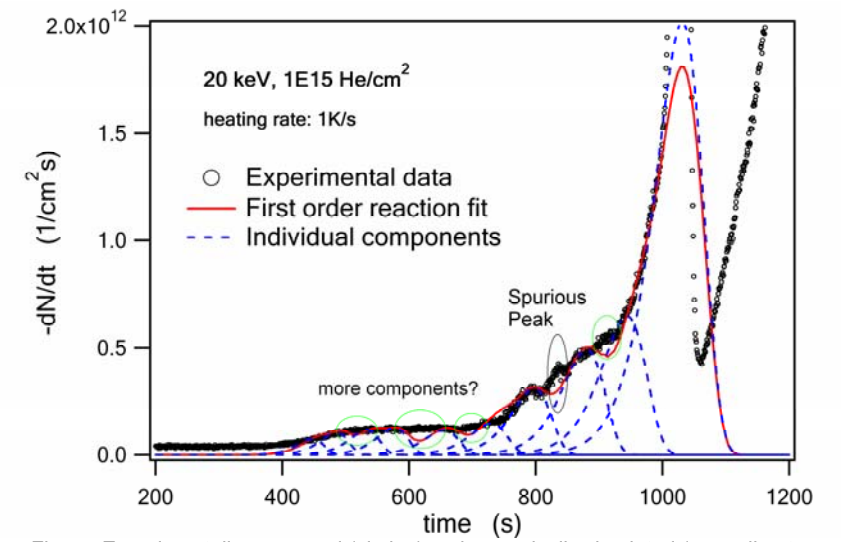

Fig. 7. Experimentally measured (circles) and numerically simulated (according to first order reaction model) (red solid line) helium desorption rates together with the individual desorption events (blue dashed line).

There are several explanations that might be possible for this non-perfect fitting of the 20 keV sample. First, the easiest explanation would be that there are more individual desorption events involved in the 20 keV sample than in the 5 keV sample. If we add in a few more individual events in our simulation, we can certainly improve the quality of the matching. Second, it may be possible that there is more contribution from spurious signal than what we have recognized. Third, but not least probable, there may be non-negligible retrapping encountered by some desorbed helium before they could reach the surfaces. One might be tempted to rule out the retrapping from possible explanations upon noticing that the simulated signal shown in Fig. 7 is actually lower than the measured signal at the mismatched spots. However it should be clarified that the relative height of the simulated and the measured signals may be reversed at mismatched spots if we change the values of initial number of atoms N_0 of the relevant components. Further investigations are required to understand this result.

Source of Non-1st-order Sharp Peak

We have seen a very similar sharp peak around 1020ºC on each of the signals recorded from the 5, 20, and 100 keV helium implanted iron samples. In the previous report [21] we have left this question unanswered: what is the source of the non-1st-order sharp peak? Putting together all the observations and analysis results, including those presented in the last report, we now believe that this sharp peak, or, more appropriately, the irregularly rapid release of helium, is due to the alpha ↔ gamma structural phase transition.

First, the repetitive appearance of this sharp peak during heating and cooling and subsequent re-heating and re-cooling (if all the implanted helium is not completely desorbed during the first cycle) resembles the reversibility of the alpha ↔ gamma phase transition very well. In fact, without the reversible phase transition, we can only expect a monotonically decreasing desorption rate without any peak during cooling process since both the reaction constant $K_0 \exp(-Q/K_B T)$ and the remaining number to be desorbed N in the rate equations of any order (for 1st order, see Eq. (6); for nth order, replace the N in Eq. (6) with N^n) decrease as temperature decreases.

Second, we have shown in the previous report that the peak sharpness can be very well reproduced using a Johnson-Mehl-Avrami kinetic model [25,26]. Considering that the JMA model is primarily applied to phase transitions, this in fact provides additional supportive evidence for the above claim. It should be pointed out that the JMA model is limited to diffusional phase transitions proceeding by nucleation and

growth and thus it can not describe diffusionless martensitic phase transitions which are often encountered in iron or ferritic alloys. However, the martensitic phase transition can occur in elemental iron only at extremely high ramping rates on the order of 10^4 K/s [27], far above the rates used in our studies. It should be mentioned that Sugano et al. [28] and Ono et al. [29] have also reported recently the observation of the non-1st-order rapid release signals from iron and certain ferritic alloys and attributed them to phase transitions, although they did not perform cooling or re-cycling studies or JMA analysis.

Having concluded that the sharp peak is due to the alpha ↔ gamma phase transition, we can then use this characteristic peak to calibrate our temperature readings at different ramping rates, and this approach is currently being carried out. For each of the interested heating rates, we measure the peak transition temperature using an accurate differential scanning calorimetry (DSC) facility and then compare with the measured temperature using our THDS system. An additional standard point for calibration, 577ºC, can be obtained by using an Al-film-on-Si-wafer eutectic reaction method.

While the calibration has not been completed at present, we have made a rough estimate for the effect of correcting temperature readings on the derived activation energies. Table 1 also lists the corrected values, Q_{corr}, of individual activation energies for the 5 keV and $1x10^{15}$ He/cm^2 sample. The Q_{corr} values were calculated from Eq. (8) using corrected peak positions. The correction to the peak positions is performed by simply subtracting 81ºC from the fitting-derived values. This 81ºC subtraction is based on the assumption that the sharp peak temperature measured as 993ºC during a heating ramp at 0.5 K/s corresponds to the literature value of the alpha ↔ gamma iron phase transition point at 912ºC. Even though this is apparently an overcorrection, it turns out that the activation energies are changed by only 0.2 or 0.3 eV.

Source of spurious peaks

It should be pointed out that all of the above experiments were performed with the sample/crucible, the filament and the thermocouple being surrounded by a molybdenum thermal shield. During a more recent experiment on a non-implanted iron sample without the presence of the thermal shield, we have observed a significant reduction in the magnitude and curvature of the total pressure as shown in Fig. 8. The He signal became quite flat with no identifiable spurious peaks until the temperature was so high as to counteract the cooling of the chamber wall (realized by flowing liquid nitrogen inside) and to begin desorbing physically-adsorbed molecular species off of the chamber wall. Meanwhile, a spurious peak still can be recognized on the total pressure and other gas signals at a common temperature.

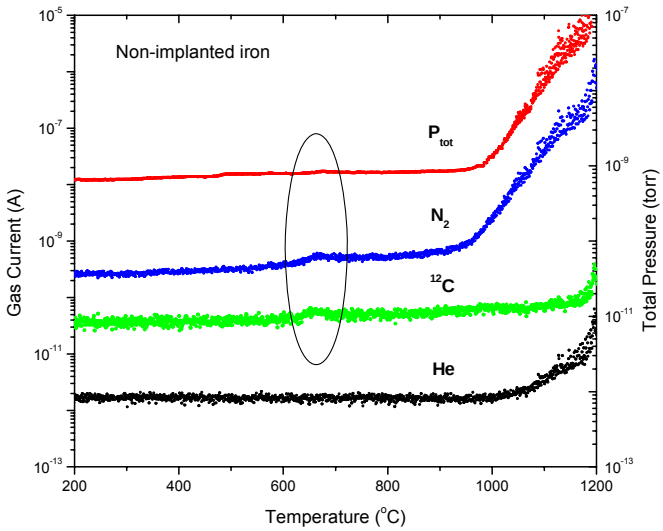

Fig. 8. Signals recorded during an experiment on a non-Implanted iron sample without the presence of thermal shield.

It appears that both the old thermal shield and the samples themselves were responsible for the appearance of the spurious peaks on He signal in previous experiments. The sample surfaces always contain physically adsorbed molecular gas species while being exposed in the open atmosphere. These molecular species can then desorb at certain temperatures and, depending on the total pressure in the system, can or can not produce spurious peaks in the helium signal. With the old thermal shield, the total pressure was quite high and consequently, the helium signal was influenced by the desorption of other species from the sample surfaces.

However, performing experiments without a thermal shield may cause other problems, e.g., non-uniform temperature distribution around the sample/crucible, and over-heating of the chamber wall. We have observed some inconsistency in temperature readings while experimenting without the shield which may be caused by large temperature gradient around the thermocouple junction. In order to get a reliable reading, the measurement junction of a thermocouple and the portion of its wires close to the junction should normally be kept at a uniformly temperature field. Therefore, instead of experimenting without a shield, it may be better to replace the old shield with a new and clean one. Efforts to improve the signal to noise ratio and to reduce the number of spurious desorption events will continue.

Conclusions

Following our previous report, we have performed new implantations at energies lower than 100 keV. Initial measurements on the new samples have revealed a large number of desorption peaks within both bcc and fcc Fe temperature ranges. The peaks in the bcc range are generally well fit with first order reaction kinetics which discloses a series of activation energies ranging from ~1.9 to ~3.5 eV. The number and the relative intensities of detected desorption peaks within the bcc temperature range appear to increase with decreasing implantation energy. The non-1st-order sharp peaks previously reported for 100 keV and 1x10^{15} He/cm^2 and also observed for the 5 keV and 1x10^{15} ion/cm^2 and 20 keV and 1x10^{15} ion/cm^2 implanted iron have been attributed to the alpha ↔ gamma phase transition. Causes for the spurious peaks reported previously are also now better understood.

Acknowledgements

This work has been supported by the Office of Fusion Energy Sciences, U.S. Department of Energy, under Grant DE-FG02-04ER54750.

References

[1] L. K. Mansur and W. A. Coghlan, J. Nucl. Mater. 119 (1983) 1.
[2] H. Ullmaier, Nucl. Fusion 24 (1984) 1039.
[3] L. K. Mansur and M. L. Grossbeck, J. Nucl. Mater. 155 (1988) 130.
[4] H. Trinkaus and B. N. Singh, J. Nucl. Mater. 323 (2003) 229.
[5] I. Mori, T. Morimoto, R. Kawakami, and K. Tominaga, Nucl. Instrum. Methods Phys. Res. Sect. B 153 (1999) 126.
[6] A. A. Selezenev, V. G. Golubev, and N. S. Ganchuk, Chem. Phys. Rep. 17 (1998) 295.
[7] K. Morishita, R. Sugano, B. D. Wirth, and T. D. de la Rubia, Nucl. Instrum. Methods Phys. Res. Sect. B 202 (2003) 76.
[8] B. D. Wirth et al., J. Nucl. Mater. 329–333 (2004) 103.
[9] L. Ventelon, B. D. Wirth, and C. Domain, J. Nucl. Mater. 351 (2006) 119.
[10] C. C. Fu and F. Willaime, Phys. Rev. B 72 (2005) 064117.
[11] F. v.d. Berg, W. V. Heugten, L. M. Caspers, and A. V. Veen, Solid State Commun. 24 (1977) 193.
[12] H. L. Heinisch, F. Gao, R. J. Kurtz, and E. A. Le, J. Nucl. Mater. 351 (2006) 141.
[13] R. J. Kurtz and H. L. Heinisch, J. Nucl. Mater. 329 (2004) 1199.
[14] F. Gao, H. Heinisch, and R. J. Kurtz, J. Nucl. Mater. 351 (2006) 133.
[15] M. B. Lewis and K. Farrell, Nucl. Instrum. Methods Phys. Res. Sect. B 16 (1986) 163.
[16] K. Arakawa, R. Imamura, K. Ohota, and K. Ono, J. Appl. Phys. 89 (2001) 4752.

[17] T. Ishizaki, Q. Xu, T. Yoshiie, and S. Nagata, Mater. Trans. 45 (2004) 9.
[18] T. Iwai, Y. Ito, and M. Koshimizu, J. Nucl. Mater. 329 (2004) 963.
[19] R. Sugano, K. Morishita, A. Kimura, H. Iwakiri, and N. Yoshida, J. Nucl. Mater. 329 (2004) 942.
[20] R. Vassen, H. Trinkaus, and P. Jung, Phys. Rev. B 44 (1991) 4206.
[21] D. Xu, T. Bus, S. C. Glade, and B. D. Wirth, Fusion Materials Semiannual Progress Report DOE/ER-0313/39 (2005) 151.
[22] S. C. Glade, B. D. Wirth, and H. Schut, Fusion Materials Semiannual Progress Report DOE/ER-0313/37 (2004) 136.
[23] J. F. Ziegler, J. P. Biersack, and U. Littmark, The Stopping and Range of Ions in Matter (Pergamon, New York, 1984).
[24] A. van Veen, A. Warnaar, and L. M. Caspers, Vacuum 30 (1980) 109.
[25] W. A. Johnson and R. F. Mehl, Trans. Am. Inst. Min. Metall. Engs. 135 (1939) 416.
[26] M. Avrami, J. Chem. Phys. 7 (1939) 1103.
[27] ASM Handbook, ASM International, Vol. 9 (2004) 148.
[28] R. Sugano, K. Morishita, and A. Kimura, Fusion Sci. Technol. 44 (2003) 446.
[29] K. Ono, K. Arakawa, H. Shibasaki, H. Kurata, I. Nakamichi, and N. Yoshida, J. Nucl. Mater. 329–333 (2004) 933.